Journal of
Materials Chemistry A

Materials for energy and sustainability

Accepted Manuscript

This article can be cited before page numbers have been issued, to do this please use: M. Cai, Y. Zhang, Y. Zhao, Q. Liu, Y. Li and G. Li, *J. Mater. Chem. A*, 2020, DOI: 10.1039/D0TA07793C.

ROYAL SOCIETY
OF **CHEMISTRY**

rsc.li/materials-a

View Article Online
DOI: 10.1039/D0TA07793C

ARTICLE

Two-dimensional metal-organic frameworks nanosheets for highly efficient electrocatalytic biomass 5-(hydroxymethyl)furfural (HMF) valorization

Received 00th January 20xx,
Accepted 00th January 20xx

DOI: 10.1039/x0xx00000x

Mengke Cai,[+a] Yawei Zhang,[+a] Yiyue Zhao,[a] Qinglin Liu,[a] Yinle Li[a] and Guangqin Li[*a]

To construct green chemical synthesis system for future life of human beings, the utilization of water as oxygen source and electricity as driving force for the oxygenation of biomass valorization is of great significance and essential. Here we firstly investigate the possibility for 5-hydroxymethylfurfural (HMF) electrooxidation into 2,5-furandicarboxylic acid (FDCA) by Ni-based two-dimensional metal-organic frameworks (2D MOFs) as electrocatalyst. FDCA is a desirable alternative to substitute fossil-based terephthalic acids for the production of environmentally friendly polymers. The as-prepared Co-doped 2D MOFs NiCoBDC (Ni^{2+}, BDC=terephthalic acid) have a high FDCA yield of 99%, excellent yield rate of 20.1 μmol cm^{-2} h^{-1} and 78.8% Faradaic efficiency at 1.55V vs RHE, as performed in electrolyte of pH 13, where the degradation of HMF could be ignored. Benefited from the accessible pores for HMF molecules, abundant exposed active sites and coupling effects between Ni and Co atoms, the 2D NiCo-MOFs realized a high catalytic activity and robust electrochemical durability. This work demonstrates 2D MOFs as a promising electrocatalysts for highly efficient biomass valorization because of their porosity and rich active sites.

Introduction

Biomass, as renewable and accessible precursor for versatile fine chemicals, exhibits promising potential to reduce the consumption of the state-of-the-art fossil fuel.[1-3] Especially, to produce value-added chemicals, utilizing the sustainable-derived electricity has attracted particular attention, which meets the demand for optimizing the energy structure of power grid.[4-6] 5-Hydroxymethylfurfural (HMF) generated by dehydrogenation of carbohydrates, classified as one of the biomass-derived platform molecules, can be derived into a series of valuable chemicals.[7,8] Among them, 2,5-furandicarboxylic acid (FDCA) can replace terephthalic acid in plastic industry to construct environment-friendly furan-based polyester with similar structure and function. Corresponding products, such as beverage bottles, textiles and food packaging have been produced on the market by the DuPont, BASF, DSM, SynbiaS, Avantium and ALPLA.[8,9]

Traditionally, most of studies of generation of FDCA focused on aerobic oxidation of HMF using heterogeneous catalysis.[10] In order to obtain highly active oxygen species, not only elevated oxygen pressure and temperature are required, but also noble metals (for example Au, Pd and Pt) have usually served as the main catalysts.[11,12] Over past decades, electrochemical oxidation of HMF drew a lot of attention.[13-17] Because compared with aerobic oxidation, the driven force can be adjusted by both potential applied on the anodic electrode and electrolyte concentrations, and ambient temperatures can serve as performed conditions. At the beginning, Grabowski et al. probed the ability of the electrochemical oxidation of HMF by $Ni(OH)_2$-covered Ni mesh,[13] achieving a low yield of only 71% and a Faradaic efficiency (FE) of 84% into FDCA in pH 14. More recently, transition metal compounds, such as Ni, Co, Fe, Mn based phosphides,[17,18] sulfides,[19,20] borides,[21,22] oxides,[23,24] hydroxides,[25,26] (oxy)hydroxides[27,28] and their composites,[29,30] have been demonstrated a high FDCA yield and FE. Besides, it is believed that flow reactor could improve the electrochemical efficiency by keeping constant substrate concentration and increasing substrate contact probability.[21,22,31] Generally, the reaction pathway relied on the applied potential and electrolyte concentrations, reveled by in situ spectroscopy such as Fourier transform infrared spectra,[21] surface-enhanced Raman spectra[30] and sum frequency generation vibrational spectra.[32]

However, there are still various challenges in terms of HMF electrooxidation into FDCA. Firstly, most of the current catalytic conditions are performed in alkaline solution with pH 14, where HMF will degrade into useless humins.[33] And the reaction kinetics and mechanism have not been clearly clarified, especially for binary or multi-metal catalysts. More importantly, reported catalysts for HMF oxidation usually were proved to

---

[a] MOE Laboratory of Bioinorganic and Synthetic Chemistry, Lehn Institute of Functional Materials, School of Chemistry, Sun Yat-Sen University, Guangzhou 510275, People's Republic of China. E-mail: liguangqin@mail.sysu.edu.cn

[+] Mengke Cai and Yawei Zhang are co-first author.

Electronic Supplementary Information (ESI) available: See DOI: 10.1039/x0xx0000x

View Article Online
DOI: 10.1039/D0TA07793C

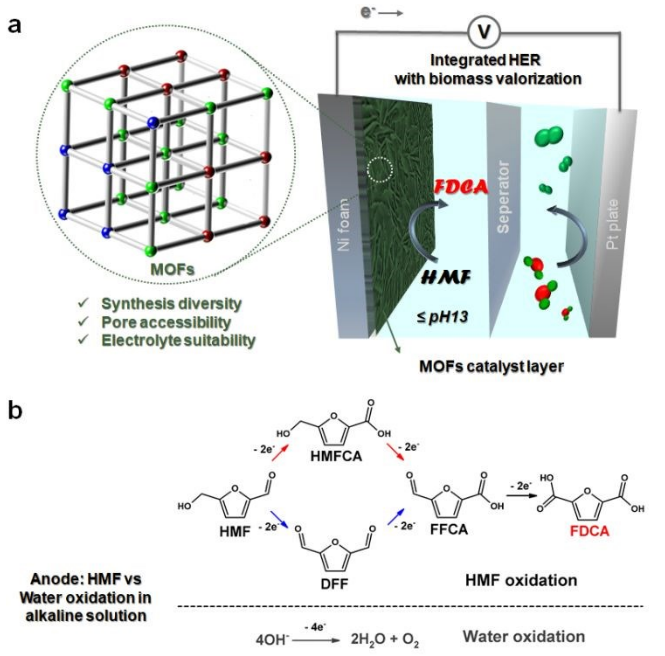

Fig.1 (a) Schematic illustration of electrocatalytic biomass HMF valorization over 2D MOFs catalyst, (b) the comparison of HMF and water oxidation pathways in alkaline solution.

exhibit good performance for water oxidation. In other words, HMF electrochemical oxidation serves as competition reaction with water oxidation in aqueous electrolyte. Thus, it is critical to balance the ability and selectivity of oxidation. Metal-organic frameworks (MOFs), as a promising platform coordination compounds, have shown great advantages and potentials in the field of electrocatalysis including synthesis diversity and pore accessibility.[34-42]

Herein, we prepared two-dimensional (2D) MOFs nanosheets grown on the nickel foam electrode, as the first case to explore the feasibility for biomass HMF valorization based on 2D MOFs (Fig. 1a). The 2D MOFs are formed by coordination of ions (Ni^{2+} or Co^{2+}) and terephthalic acid (BDC) ligands, which are good candidates for electrochemical water oxidation integrated with ions doping, ligand exchange and layer exfoliation.[35,43-46] Our recent works found that appropriate metals and ligands doping can promote the formation of high valence nickel species, and adjust the structure of d-band electron, so as to improve the electrooxidation activity.[43] To optimize the competitive reactions shown in Fig. 1b, we can take the strategy of stabilizing the high valence of Ni ions by Co-doped to improve the FE for HMF oxidation. Furthermore, 2D MOFs can supply enough channels for the diffusion of biomass HMF and its products, larger than water molecules in size.

Results and discussion

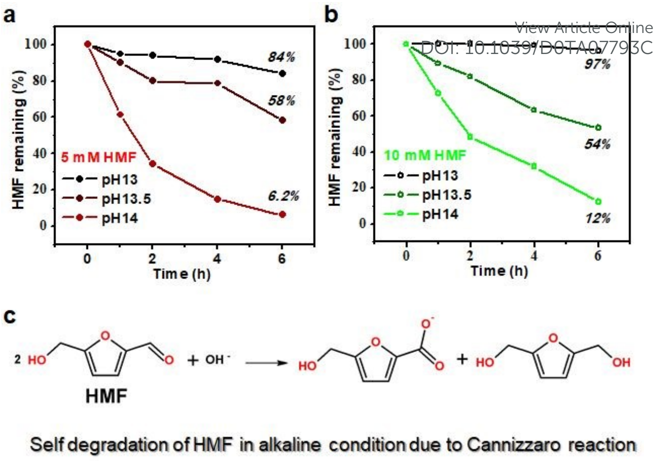

Fig.2 Stability tests of (a) 5 mM and (b) 10 mM of HMF in different alkaline solutions under room temperature and ambient pressure, without stirring during 6 h test. (c) Possible self-degradation mechanism due to Cannizzaro reaction.

It is noticed whether it is homogeneous catalysis, heterogeneous catalysis or electrocatalysis for HMF oxidation, the oxidation reaction generally relies on alkaline conditions.[33,47,48] As mentioned in introduction, HMF is not stable in high pH solution. In the early stage of this research, we found that the repeatability of test data was very poor when using 20 mL of pH 14 aqueous solution with 10 mM of HMF. Considering the lab-scale electrolysis with a dilute and small volume HMF solution, the effect of high pH had been a key factor to influence the stability of HMF and data accuracy. Hence, we investigated above two effects on the stability of HMF with high performance liquid chromatography (HPLC) analysis (Fig. S1-2). Fig. 2 showed the comparison of HMF remaining with different substrate concentrations and pH conditions. Without stirring, the 5 and 10 mM of HMF kept only 6.2% and 12%, where large amounts of HMF degraded due to strong alkaline environment. We noted that the more alkaline electrolyte, the more unstable HMF. At pH 13 for a 10 mM HMF solution, the loss became rarely negligible during 6 h. This phenomenon is mainly attributed to the self-oxidation-reduction of HMF, as an aromatic aldehyde without α-hydrogen atom, *via*

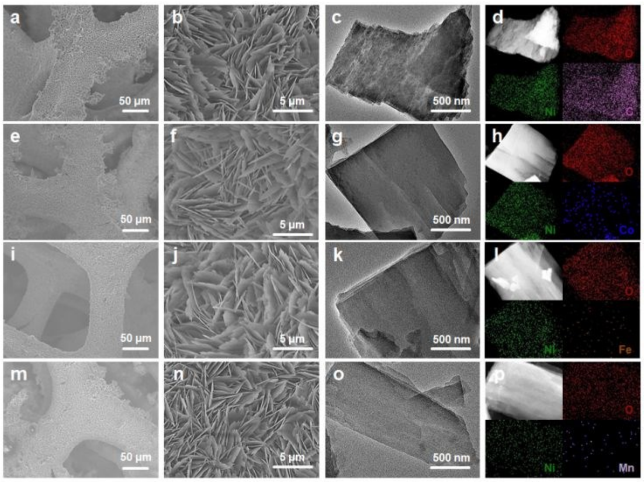

Fig.3 Scanning electron microscopy (SEM), transmission electron microscopy (TEM) and elemental mapping images of the as-synthesized (a-d) NiBDC-NF, (e-h) NiCoBDC-NF, (i-l) NiFeBDC-NF and (m-p) NiMnBDC-NF.

View Article Online
DOI: 10.1039/D0TA07793C

Cannizzaro reaction at high ratio of OH^- to HMF. This finding illustrates that HMF oxidation tests should be performed at as low alkaline conditions as possible. As MOFs-based catalysts usually showed weak stability in long-term electrocatalytic process,[34-36,43-46] thus here lower alkaline electrolyte pH 13 was chosen for electrooxidation conditions of HMF.

The synthetic processes of NiBDC-NF and binary NiMBDC-NF (M = Co, Fe, Mn) are described in the experiment section in supporting information, and nickel foam (NF) serves as not only current collector, but also growth substrate for 2D MOFs nanosheets. Then the structural characteristics were studied by X-ray diffraction (XRD). As shown in Fig. S3a, the main peak at 10° of NiBDC was relatively weak compared with the two main peaks of NF at 45° and 52°. When removed from NF substrate, all specimens exhibited strong diffraction peaks (Fig. S3b), indicating good crystallinity and partial doping did not change the pristine NiBDC phase. Afterwards, nitrogen adsorption-desorption was conducted to evaluate specific surface area and pore size distribution (Fig. S4 and Table S1). Both NiCoBDC and NiFeBDC possessed larger specific surface area and pore volume, besides adsorption-desorption hysteresis loop appeared. It meant that both above specimens could provide more accessible reaction sites and hierarchical pore environment for biomass electrooxidation.

The morphologies of the NiBDC-NF and other doping specimens are shown in Fig. 3, which all exhibited the same nanostructure characteristics. NiBDC nanosheets could grow vertically and uniformly on the NF by solvothermal strategy, exposing enough surface and pore (Fig. 3a, b). TEM images proved that the NiBDC showed 2D morphology with a micron-level lateral dimension (Fig. 3c). The 2D morphology is derived from the special crystal structure, which is composed of $[NiO_6]$ octahedral layer and terephthalic acid along a axis (Fig. S5).[49] When BDC ligands dissociate, NiBDC will form 2D sheets with b, c axis as the plane.[35,44] After introducing partial metals doping into NiBDC, pristine 2D morphology remained, and doped metal elements (Co, Fe, Mn) could dispersed uniformly with Ni and O (Fig. 3e-p). To further examine the composition of doped elements, energy-dispersive X-ray spectroscopy (EDS) was applied, and the Ni/metal-doped ratios were 10:1 (Ni/Co), 9.5:1 (Ni/Fe) and 10:1 (Ni/Mn) shown in Table S2. The results were close to the feed ratio of 9:1 in the synthetic step.

The electrocatalytic performance of all specimens for HMF oxidation were studied by three-electrode setup, and pH was set at 13 during all tests. As shown in Fig. 4a, the activity of pristine NiBDC-NF was investigated by linear sweep voltammetry (LSV). To drive a current density of 10 mA cm^{-2}, the applied potential for HMF oxidation was about 210 mV lower than that for water oxidation, indicating that the oxidation of HMF was more favorable on the NiBDC-NF. More interestingly, the oxidation peak of Ni^{2+} to Ni^{3+} vanished in the presence of HMF (10 mM), usually regarded as the activation process of Ni-based water oxidation electrocatalysts.[21,27,50] The main reason was that Ni oxidation feature might be overlaid by the current of HMF oxidation. The formation of the high oxidation state of Ni, in this case Ni^{3+}, was consumed rapidly to oxidize HMF and no obvious redox peak could be observed. To compare the electrochemical surface area (ECSA), which can characterize the active sites of the electrocatalysis, Δj at 1.42 V (vs

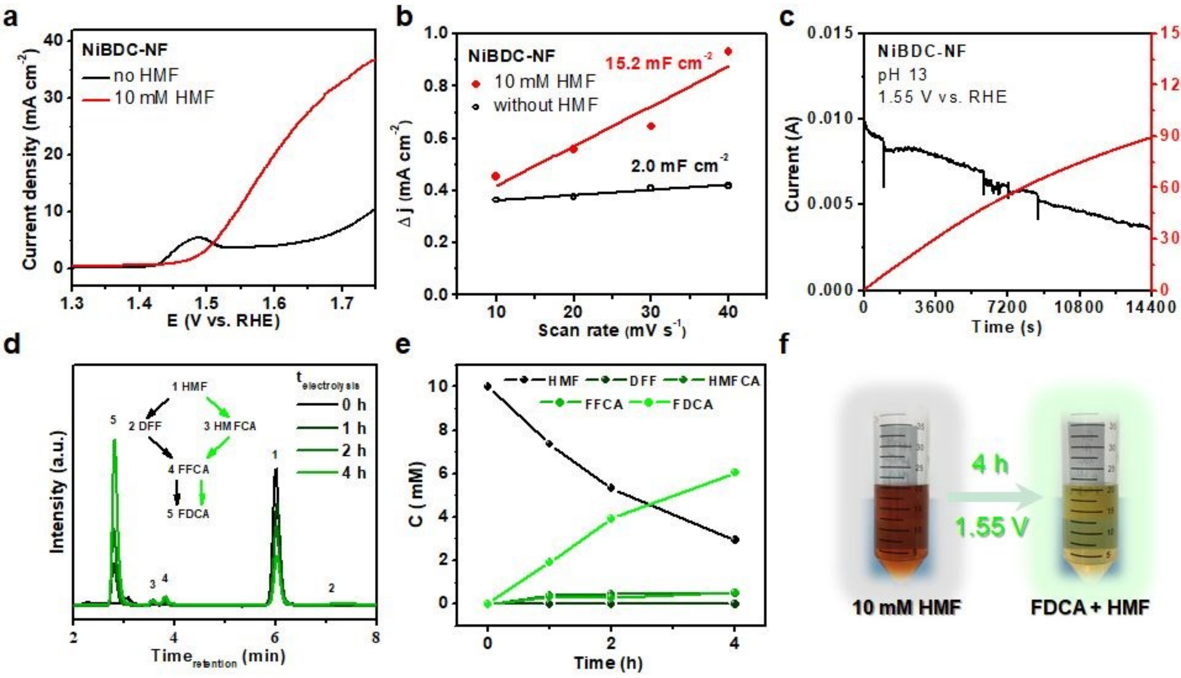

Fig.4 (a) The LSV for the NiBDC-NF at a scan rate of 5 mV s^{-1} in 0.1 M KOH without and with 10 mM HMF. (b) Corresponding change of current density plotted against scan rates without and with 10 Mm HMF. (c) Current-time and charge-time plots during constant potential (1.55 V vs RHE) electrolysis using NiBDC-NF. (d) HPLC chromatogram at various electrolysis times. (e) Concentrations of HMF and the oxidation products at different electrolysis time. (f) Comparison of the HMF solution before and after electrolysis.

View Article Online
DOI: 10.1039/D0TA07793C

RHE) was plotted with different scan rates to gain the double-layer capacitance (C_{dl}).[51] After introducing 10 mM HMF into 0.1 M KOH, the C_{dl} values increased from 2.0 to 15.2 mF cm^{-2}, indicating that there were more reactive sites for HMF (Fig. 4b). Similarly, the Co,Fe,Mn-doped NiBDC-NF showed the same electrocatalytic properties, as shown in Fig. S6-7. Based on above results, constant potential electrolysis was conducted over pristine NiBDC-NF at 1.55 V vs RHE for 4 h. As electrolysis proceeded, the current density sharply decreased due to the consumption of HMF, while the transferred charge kept linear increase (Fig. 4c). Continuously monitored by HPLC, the reaction process was clearly demonstrated with exact pathway, as shown in Fig. 4d. Using NiBDC-NF as catalyst, the HMF concentration decreased while FDCA increased. And there was no dialdehyde 2,5-diformylfuran (DFF) detected as mediates during the total reaction period. Unfortunately, the electrooxidation of HMF could not be completed within 4 h over pristine NiBDC-NF, showing a yield of only about 60% (Fig. 4e). The comparison of the HMF solution before and after electrolysis also proved it was an incomplete transformation over the NiBDC-NF at 1.55 V in 4 h (Fig. 4f). In view of the above results, there were two highlight points. The one was that FDCA is generated by NiBDC-NF catalyst, following the route of 5-hydroxymethyl-2-furancarboxylic acid (HMFCA) rather than the route of DFF formation. Another was that the catalytic performance was still modest over the pristine NiBDC-NF, so it was necessary to optimize the performance by doping engineering or adjusting the applied potential.

To further verify the HMF oxidation activity of as-prepared 2D MOFs specimens, applied potential and electrolysis time were employed to investigate the FE and FDCA yield rate (Fig. S8-10). As shown in Fig. 5a-d and Table S3, the higher applied potential, the higher FDCA yield rate, while the lower FE for these catalysts. It meant that high yield rate and FE could not be achieved at the same time. Encouragingly, it was obvious that Co-doped NiBDC-NF, named as NiCoBDC-NF, showed a comparable and superior yield rate and FE, in contrast with other three catalysts. Moreover, the electrolysis time played a key role in catalytic performance. Consistent with above current-time plots in Fig. 4c, total FDCA yield rate decreased as electrolysis continued, implying that flow reactor did act as a key process strategy for industrialization of HMF electrooxidation. Based on 4 h catalytic results, the highest yield rate of 20.1 μmol cm^{-2} h^{-1} (a yield of 99%) was achieved at 1.55V vs RHE, while the FE of 78.8% was obtained. The catalytic performance was comparable with most of reported electrocatalysts performed in electrolyte with pH conditions less than 14 (Table S4).[14-16,23,24,27,33,52,53] Subsequently, the Tafel plots were determined (Fig. 5e). The NiCoBDC-NF possessed a Tafel slope of 60.8 mV dec^{-1} in the presence of HMF, lower than that of other specimens, suggesting the superior kinetic process of Co-doped specimen for HMF electrooxidation.

The stability is an important factor in evaluating the electrocatalytic performance, especially MOF-based electrocatalysts usually perform a modest stability due to weaker coordination bond than ionic and covalent bond.[54,55] As shown in Fig. S11-12, NiBDC-NF and NiCoBDC-NF could maintain the original crystallinity with only a little decrease, conducted on the potential of 1.45 and 1.55 V, and the color of specimen images did not change into black, suggesting both specimens exhibited superior stability compared with NiFeBDC-NF and NiMnBDC-NF. Notably, Fe-doped specimen NiFeBDC-NF showed poor stability even if the voltage of 1.45 V was applied, indicating that Fe-doped NiBDC was not suitable to apply in HMF oxidation. On the contrary, to assess the durability of the best catalyst NiCoBDC-NF, four successive electrolysis were conducted at the constant potential of 1.55 V vs RHE. As seen in Fig. 5f, the FE and selectivity of HMF into FDCA could be maintained around 79% and 95%, respectively. And the yield rate decreased to 16.4 from 20.1

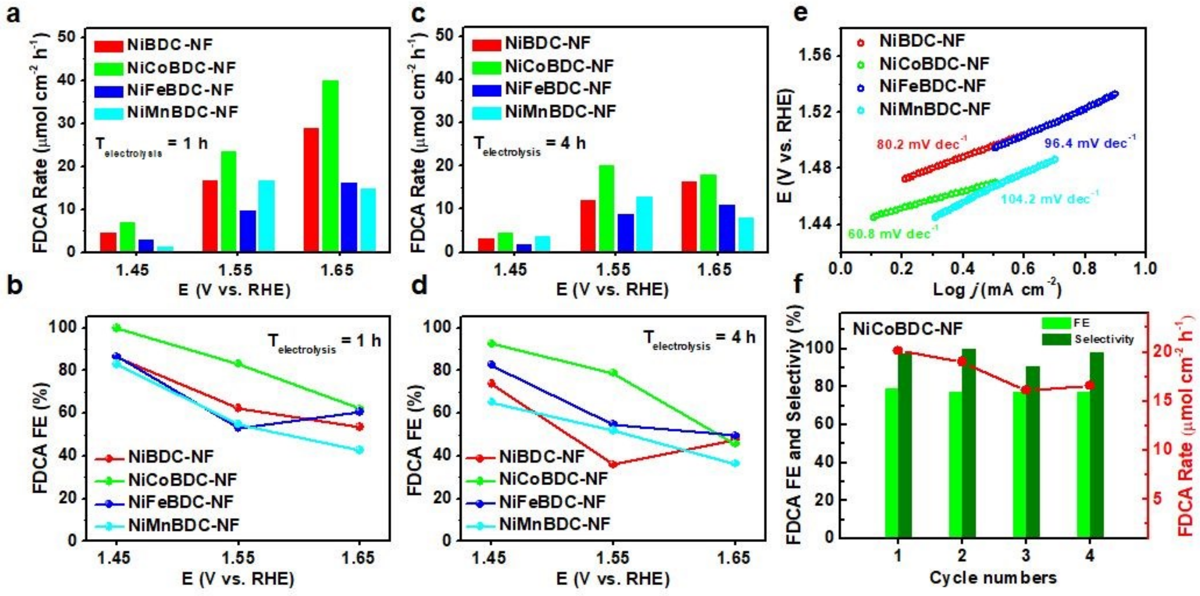

Fig.5 FDCA yield rate and FE of NiBDC, NiCoBDC, NiFeBDC and NiMnBDC for (a,b) 1 h and (c,d) 4h electrolysis. (e) Tafel plots in the presence of HMF. (f) FE, selectivity and yield rate of FDCA using NiCoBDC-NF during four successive electrolysis.

View Article Online
DOI: 10.1039/D0TA07793C

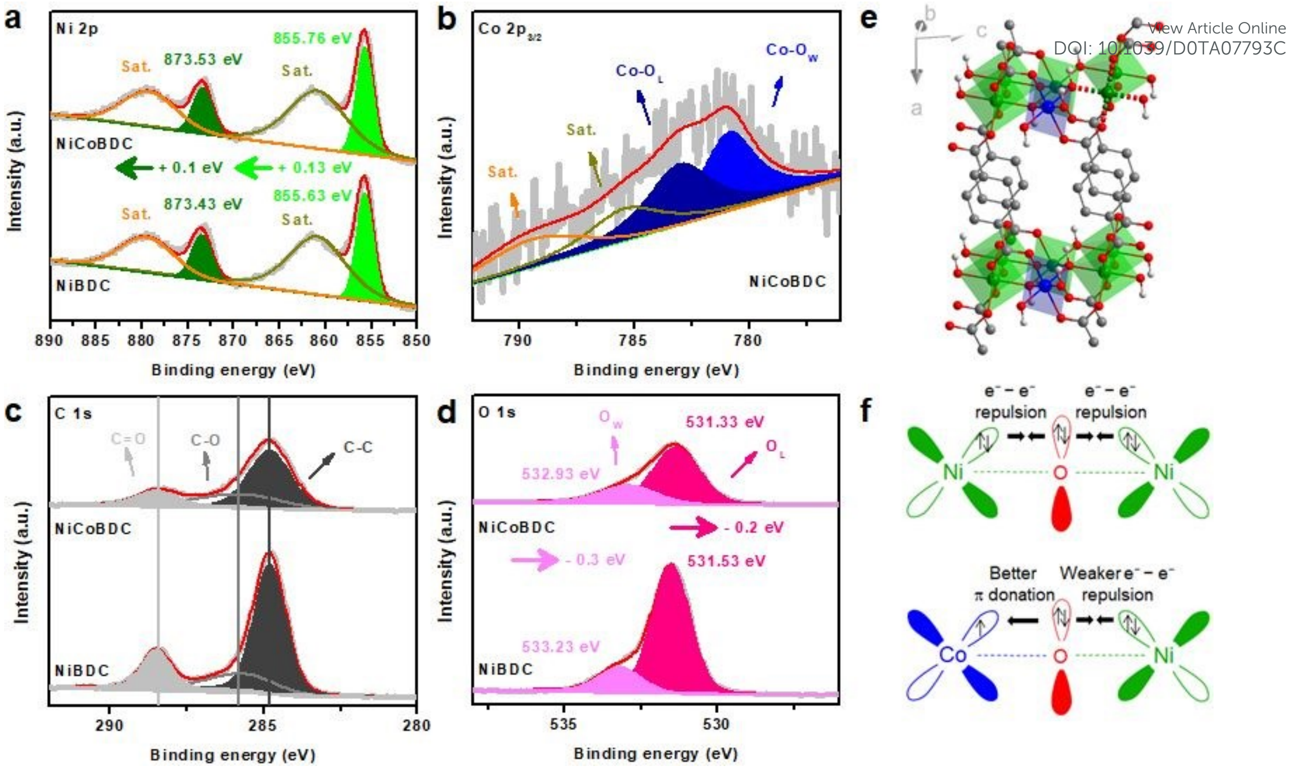

Figure 6. Electronic structure characterization of NiBDC-NF and NiCoBDC-NF. (a) Ni 2p, (b) Co $2p_{3/2}$, (c) C 1s and (d) O 1s of specimens. (e) The coordinatively unsaturated sites model for the Ni atom on the surface of NiCoBDC-NF. (f) Schematic representation of the electronic coupling between Ni and Co in NiBDC-NF and NiCoBDC-NF.

μmol cm^{-2} h^{-1} with a slight attenuation. Moreover, the crystallinity of post NiCoBDC-NF also could maintain, and the morphology and elemental distribution showed limited changes after four successive cycle electrocatalysis (Fig. S13).

Moreover, the X-ray photoelectron spectroscopy (XPS) was carried out to understand the electronic states of Co-doped NiCoBDC-NF and pristine NiBDC-NF.[56] It was meaningful why did Co-doped NiBDC-NF perform better in catalytic activity. Compared with the NiBDC, the peaks of Ni $2p_{3/2}$ and Ni $2p_{1/2}$ in the high-resolution Ni 2p spectrum of the NiCoBDC shifted to a higher binding energy (Fig. 6a), a shift of 0.13 and 0.1 eV, respectively. This revealed that the local electronic structure of Ni^{2+} was modified.[57,58] After the hybridization, the Co^{2+} was introduced into the sites of Ni^{2+} in NiBDC crystal cell. Fig. 6b showed the XPS in the Co $2p_{3/2}$ region. Two strong peaks at 780.78 and 782.88 eV could be assigned to Co-O_W and Co-O_L, associated with two satellite peaks. From the structural point of view, the Co-O bonds involved the oxygen atoms in coordinated H_2O (O_W) and ligands containing oxygen (O_L) such as μ-OH and carboxyl (Fig. 6e). The C 1s spectrum (Fig. 6c) was divided into three peaks. The peak at 284.83 eV was the standard C-C as the reference, while the peaks at 286.23 and 288.58 eV corresponded to the C-O and C=O.[59] Interestingly, the peaks located at 531.33 and 532.93 eV in the O 1s spectrum of NiCoBDC exhibited negative shifts,[60] compared with 531.53 and 533.23 eV in the pristine NiBDC, as shown in Fig. 6d. Thus, this reflected a partial electron was transferred from Ni^{2+} to O^{2-}, which was explained well in terms of their electronic structure (Fig. 6f). The valence electronic configuration of Ni^{2+} was $3d^8$, and its π-symmetry (t_{2g}) d-orbital were fully occupied. Thus, the major interaction between Ni^{2+} and bridging O^{2-} was e^--e^- repulsion, hindering the charge transfer. After introducing Co^{2+}, the unpaired electrons in the π-symmetry (t_{2g}) d-orbital could interact with bridging O^{2-} *via* π-donation, weakening the e^--e^- repulsion and promoting partial charge transfer from Ni^{2+} to Co^{2+}, as implied by the above XPS analysis.[61-63] These results clearly demonstrated that the coupling between Ni^{2+} and Co^{2+} could boost the formation of high valence nickel species, which was considered as the catalytic sites for the oxidation of organic alcohols and aldehydes.[64-66]

Conclusions

In summary, a series of 2D Ni-MOFs with metal-doped (Co, Fe, Mn) have been successfully synthesized by solvothermal method, and then firstly served as electrocatalysts for the HMF electrooxidation into FDCA in a pH 13 medium. Notably, strong alkalinity, such as pH 14, was found to be not suitable as electrocatalytic conditions, which accelerated the degradation of HMF, thus overestimating the electrochemical performance. And the Co-doped NiCoBDC-NF showed excellent activity, selectivity and stability for the HMF electrooxidation, with a high FDCA yield rate of 20.1 μmol cm^{-2} h^{-1}, excellent yield of 99%, a faradaic efficiency of 78.8% and four successive catalytic cycles at 1.55V vs RHE. It was contributed to the optimized electronic structure with Co-doped, high valence of Ni formed easily in the 2D MOFs, which was regarded as the active sites for the oxidation of aldehydes and alcohols. Our study significantly advances research towards biomass valorization, and stimulates extensive exploration of 2D MOFs for electrocatalysis and beyond.

Conflicts of interest

The authors declare no conflict of interest.

Acknowledgements

This work was supported by the Overseas High-level Talents Plan of China and Guangdong Province, and the 100 Talents Plan Foundation of Sun Yat-sen University, the Fundamental Research Funds for the Central Universities, the Program for Guangdong Introducing Innovative and Entrepreneurial Teams (2017ZT07C069), the Fundamental Research Funds for the Central Universities, and the NSFC Projects (21821003 and 21890380).

Notes and references

1 N. S. Lewis and D. G. Nocera, *Proc. Natl. Acad. Sci. U. S. A.*, 2006, **103**, 15729–15735.
2 A. Corma, S. Iborra and A. Velty, *Chem. Rev.*, 2007, **107**, 2411-2502.
3 D. R. Dodds and R. A. Gross, *Science*, 2007, **318**, 1250-1251.
4 J. J. Bozell, *Science*, 2010, **329**, 522.
5 B. A. Frontana-Uribe, R. D. Little, J. G. Ibanez, A. Palma and R. Vasquez-Medrano, *Green Chem.*, 2010, **12**, 2099-2119.
6 S. Xu, P. Zhou, Z. Zhang, C. Yang, B. Zhang, K. Deng, S. Bottle and H. Zhu, *J. Am. Chem. Soc.*, 2017, **139**, 14775-14782.
7 J. J. Bozell and G. R. Petersen, *Green Chem.*, 2010, **12**, 539-554.
8 R.-J. van Putten, J. C. van der Waal, E. de Jong, C. B. Rasrendra, H. J. Heeres and J. G. de Vries, *Chem. Rev.*, 2013, **113**, 1499-1597.
9 C. Xu, E. Paone, D. Rodriguez-Padron, R. Luque and F. Mauriello, *Chem. Soc. Rev.*, 2020, **49**, 4273-4306.
10 X. Zuo, P. Venkitasubramanian, D. H. Busch and B. Subramaniam, *ACS Sustainable Chem. Eng.*, 2016, **4**, 3659-3668.
11 Z. Zhang and K. Deng, *ACS Catal.*, 2015, **5**, 6529–6544.
12 T. Pasini, M. Piccinini, M. Blosi, R. Bonelli, S. Albonetti, N. Dimitratos, J. A. Lopez-Sanchez, M. Sankar, Q. He, C. J. Kiely, G. J. Hutchings and F. Cavani, *Green Chem.*, 2011, **13**, 2091–2099.
13 G. Grabowski, J. Lewkowski and R. Skowroński, *Electrochim. Acta*, 1991, **36**, 1995.
14 K. R. Vuyyuru and P. Strasser, *Catalysis Today*, 2012, **195**, 144-154.
15 D. J. Chadderdon, L. Xin, J. Qi, Y. Qiu, P. Krishna, K. L. More and W. Li, *Green Chem.*, 2014, **16**, 3778-3786.
16 H. G. Cha and K. S. Choi, *Nat. Chem.*, 2015, **7**, 328-333.
17 N. Jiang, B. You, R. Boonstra, I. M. Terrero Rodriguez and Y. Sun, *ACS Energy Lett.*, 2016, **1**, 386-390.
18 B. You, N. Jiang, X. Liu and Y. Sun, *Angew. Chem., Int. Ed.*, 2016, **55**, 9913-9917.
19 B. You, X. Liu, N. Jiang and Y. Sun, *J. Am. Chem. Soc.*, 2016, **138**, 13639-13646.
20 X. Deng, X. Kang, M. Li, K. Xiang, C. Wang, Z. Guo, J. Zhang, X.-Z. Fu and J.-L. Luo, *J. Mater. Chem. A*, 2020, **8**, 1138-1146.
21 S. Barwe, J. Weidner, S. Cychy, D. M. Morales, S. Dieckhofer, D. Hiltrop, J. Masa, M. Muhler and W. Schuhmann, *Angew. Chem., Int. Ed.*, 2018, **57**, 11460-11464.
22 J. Weidner, S. Barwe, K. Sliozberg, S. Piontek, J. Masa, U. P. Apfel and W. Schuhmann, *Beilstein J. Org. Chem.*, 2018, **14**, 1436-1445.
23 L. Gao, Y. Bao, S. Gan, Z. Sun, Z. Song, D. Han, F. Li and L. Niu, *ChemSusChem*, 2018, **11**, 2547-2553.
24 S. R. Kubota and K. S. Choi, *ChemSusChem*, 2018, **11**, 2138-2145.
25 W.-J. Liu, L. Dang, Z. Xu, H.-Q. Yu, S. Jin and G. W. Huber, *ACS Catal.*, 2018, 8, 5533-5541.
26 D. J. Chadderdon, L. P. Wu, Z. A. McGraw, M. Panthani and W. Li, *ChemElectroChem*, 2019, **6**, 3387-3392.
27 B. J. Taitt, D.-H. Nam and K.-S. Choi, *ACS Catal.*, 2018, **9**, 660-670.
28 S. Li, X. Sun, Z. Yao, X. Zhong, Y. Cao, Y. Liang, Z. Wei, S. Deng, G. Zhuang, X. Li and J. Wang, *Adv. Funct. Mater.*, 2019, **29**, 1904780.
29 L. Gao, Z. Liu, J. Ma, L. Zhong, Z. Song, J. Xu, S. Gan, D. Han and L. Niu, *Appl. Catal., B*, 2020, **261**, 118235.
30 N. Heidary and N. Kornienko, *Chem. Sci.*, 2020, **11**, 1798-1806.
31 R. Latsuzbaia, R. Bisselink, A. Anastasopol, H. van der Meer, R. van Heck, M. S. Yagüe, M. Zijlstra, M. Roelands, M. Crockatt, E. Goetheer and E. Giling, *J. Appl. Electrochem.*, 2018, **48**, 611-626.
32 N. Zhang, Y. Zou, L. Tao, W. Chen, L. Zhou, Z. Liu, B. Zhou, G. Huang, H. Lin and S. Wang, *Angew. Chem., Int. Ed.*, 2019, **58**, 15895-15903.
33 D.-H. Nam, B. J. Taitt and K.-S. Choi, *ACS Catal.*, 2018, **8**, 1197-1206.
34 Y. Xu, B. Li, S. Zheng, P. Wu, J. Zhan, H. Xue, Q. Xu and H. Pang, *J. Mater. Chem. A*, 2018, **6**, 22070-22076.
35 M. Cai, Q. Liu, Z. Xue, Y. Li, Y. Fan, A. Huang, M.-R. Li, M. Croft, T. A. Tyson, Z. Ke and G. Li, *J. Mater. Chem. A*, 2020, **8**, 190-195.
36 Y. T. Xu, Z. M. Ye, J. W. Ye, L. M. Cao, R. K. Huang, J. X. Wu, D. D. Zhou, X. F. Zhang, C. T. He, J. P. Zhang and X. M. Chen, *Angew. Chem., Int. Ed.*, 2019, **58**, 139-143.
37 C. Xu, R. Fang, R. Luque, L. Chen and Y. Li, *Coord. Chem. Rev.*, 2019, **388**, 268-292.
38 M.-R. Liu, Q.-L. Hong, Q.-H. Li, Y. Du, H.-X. Zhang, S. Chen, T. Zhou and J. Zhang, *Adv. Funct. Mater.*, 2018, **28**, 1801136.
39 F. Chen, K. Shen, J. Chen, X. Yang, J. Cui and Y. Li, *ACS Cent. Sci.*, 2019, **5**, 176-185.
40 R. Fang, A. Dhakshinamoorthy, Y. Li and H. Garcia, *Chem. Soc. Rev.*, 2020, **49**, 3638-3687.
41 P. Shao, L. Yi, S. Chen, T. Zhou and J. Zhang, *J. Energy Chem.*, 2020, **40**, 156-170.
42 Y. Wang, W. Zhan, Z. Chen, J. Chen, X. Li and Y. Li, *ACS Catal.*, 2020, **10**, 7177-7187.
43 Z. Xue, Y. Li, Y. Zhang, W. Geng, B. Jia, J. Tang, S. Bao, H.-P. Wang, Y. Fan, Z.-W. Wei, Z. Zhang, Z. Ke, G. Li and C.-Y. Su, *Adv. Energy Mater.*, 2018, **8**, 1801564.
44 S. Zhao, Y. Wang, J. Dong, C.-T. He, H. Yin, P. An, K. Zhao, X. Zhang, C. Gao, L. Zhang, J. Lv, J. Wang, J. Zhang, A. M. Khattak, N. A. Khan, Z. Wei, J. Zhang, S. Liu, H. Zhao and Z. Tang, *Nat. Energy*, 2016, **1**, 16184.
45 W. Cheng, X. Zhao, H. Su, F. Tang, W. Che, H. Zhang and Q. Liu, *Nat. Energy*, 2019, **4**, 115–122.
46 Z. Xue, K. Liu, Q. Liu, Y. Li, M. Li, C. Y. Su, N. Ogiwara, H. Kobayashi, H. Kitagawa, M. Liu and G. Li, *Nat. Commun.*, 2019, **10**, 5048.
47 Z. Zhang and G. W. Huber, *Chem. Soc. Rev.*, 2018, **47**, 1351-1390.
48 M. Sajid, X. Zhao and D. Liu, *Green Chem.*, 2018, **20**, 5427-5453.

View Article Online
DOI: 10.1039/D0TA07793C

49 A. Mesbah, P. Rabu, R. Sibille, S. Lebegue, T. Mazet, B. Malaman and M. Francois, *Inorg. Chem.*, 2014, **53**, 872-881.
50 M. Cai, Q. Liu, Y. Zhao, Z. Wang, Y. Li and G. Li, *Dalton Trans.*, 2020, **49**, 7436-7443.
51 M. Zhang, Y. Liu, B. Liu, Z. Chen, H. Xu and K. Yan, *ACS Catal.*, 2020, **10**, 5179-5189.
52 X. H. Chadderdon, D. J. Chadderdon, T. Pfennig, B. H. Shanks and W. Li, *Green Chem.*, 2019, **21**, 6210-6219.
53 A. C. Cardiel, B. J. Taitt and K.-S. Choi, *ACS Sustainable Chem. Eng.*, 2019, **7**, 11138-11149.
54 Z. Fang, B. Bueken, D. E. De Vos and R. A. Fischer, *Angew. Chem., Int. Ed.*, 2015, **54**, 7234-7254.
55 B. Li, M. Chrzanowski, Y. Zhang and S. Ma, *Coord. Chem. Rev.*, 2016, **307**, 106-129.
56 M. Cai, Y. Li, Q. Liu, Z. Xue, H. Wang, Y. Fan, K. Zhu, Z. Ke, C.-Y. Su and G. Li, *Adv. Sci.*, 2019, **6**, 1802365.
57 L. Xu, Q. Jiang, Z. Xiao, X. Li, J. Huo, S. Wang and L. Dai, *Angew. Chem., Int. Ed.*, 2016, **55**, 5277–5281.
58 Y. Liang, Y. Li, H. Wang, J. Zhou, J. Wang, T. Regier and H. Dai, *Nat. Mater.*, 2011, **10**, 780–786.
59 P. Wen, P. Gong, J. Sun, J. Wang and S. Yang, *J. Mater. Chem. A*, 2015, **3**, 13874–13883.
60 H. Guo, Z. Zheng, Y. Zhang, H. Lin and Q. Xu, *Sens. Actuators, B*, 2017, **248**, 430–436.
61 J. Y. Chen, L. Dang, H. Liang, W. Bi, J. B. Gerken, S. Jin, E. E. Alp and S. S. Stahl, *J. Am. Chem. Soc.*, 2015, **137**, 15090-15093.
62 M. Gong, Y. Li, H. Wang, Y. Liang, J. Z. Wu, J. Zhou, J. Wang, T. Regier, F. Wei and H. Dai, *J. Am. Chem. Soc.*, 2013, **135**, 8452-8455.
63 F. Song and X. Hu, *Nat. Commun.*, 2014, **5**, 4477.
64 M. W. Louie and A. T. Bell, *J. Am. Chem. Soc.*, 2013, **135,** 12329-12337.
65 Z. Xue, X. Li, Q. Liu, M. Cai, K. Liu, M. Liu, Z. Ke, X. Liu and G. Li, *Adv. Mater.*, 2019, **31**, 1900430.
66 X. Zhang, Y. Zhao, Y. Zhao, R. Shi, G. I. N. Waterhouse and T. Zhang, *Adv. Energy Mater.*, 2019, **9**, 1900881.

View Article Online
DOI: 10.1039/D0TA07793C

Table of Contents

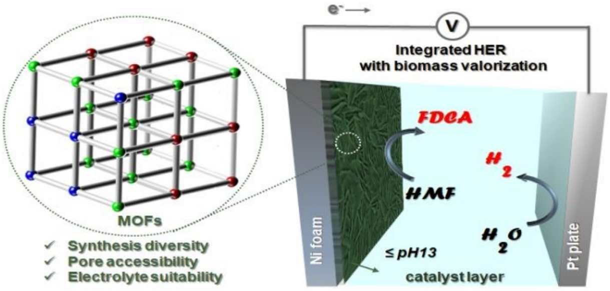

Co-doped 2D metal-organic frameworks (MOFs) could promote biomass valorization, the electrooxidation of 5-(hydroxymethyl)furfural (HMF) into 2,5-furandicarboxylic acid (FDCA), with highly efficient electrocatalytic performance due to formation of high valence of Ni, pore accessibility and electrolyte suitability.